buildings

MDPI

Article

Strength Prediction of Smart Cementitious Materials Using a Neural Network Optimized by Particle Swarm Algorithm

Pengfei Zhang [1], Fan Kong [2] and Lu Hai [3,*]

[1] College of Civil Engineering, Suzhou University of Science and Technology, Suzhou 215011, China; zhangpf@usts.edu.cn
[2] School of Civil Engineering, Hefei University of Technology, Hefei 230009, China; kongfan@hfut.edu.cn
[3] School of Engineering, Ocean University of China, Qingdao 266100, China
* Correspondence: tjhailu@163.com

Abstract: Because of the improved physical, mechanical and crack–resistant properties, smart cementitious materials have garnered significant attention in civil engineering. However, the method of predicting performance of smart cementitious materials remains a formidable task. To address this issue, this study develops a neural network optimized by particle swarm algorithm, specifically designed for predicting the strength of smart cementitious materials. Particle swarm optimization is used to determine the initial weights and biases of the neural network in this algorithm. Two types of smart cementitious materials, namely 3D printed fiber reinforced concrete and graphene nanoparticles–reinforced cementitious composites, are studied as examples. Utilizing the PSO–BPNN method and data gathered from the existing articles, the predictive models for the mechanical properties of these materials are developed. Five commonly used statistical metrics are applied to evaluate the predictive performance. The results indicate suggest the PSO–BPNN outperforms the traditional back propagation neural network. Thus, a reliable and robust performance predictive model can be built for smart cementitious materials using the proposed approach.

Keywords: compressive strength prediction; neural network; particle swarm optimization; smart cementitious materials; statistical metrics

Citation: Zhang, P.; Kong, F.; Hai, L. Strength Prediction of Smart Cementitious Materials Using a Neural Network Optimized by Particle Swarm Algorithm. *Buildings* **2024**, *14*, 2033. https://doi.org/10.3390/buildings14072033

Academic Editor: Abdelhafid Khelidj

Received: 12 April 2024
Revised: 22 June 2024
Accepted: 28 June 2024
Published: 3 July 2024

1. Introduction

Cementitious materials have gained widespread use in construction engineering due to their high compressive strength, good durability, straightforward production process and low cost [1,2]. Nevertheless, due to the weak interfaces between aggregates and mortar at mesoscale, cementitious materials commonly exhibit low tensile strength, high cracking tendency and pronounced brittleness [3,4]. The characteristic of cementitious materials that are vulnerable to cracking can compromise the load–bearing capacity and integrity of engineering structures, presenting a serious threat to their safety and reliability [5,6]. Particularly, these issues become more pronounced in the context of large–scale, complex structures subjected to extreme environmental conditions and multi–physics field coupling. Given these challenges, smart cementitious materials, which have excellent mechanical properties and multifunctional behaviors, have gained significant attention over the past few years for their potential to improve the overall performance of complex structures [7–9].

Smart cementitious materials represent a new generation of construction materials that have improved performance characteristics, including strength, durability, and adaptability to environmental changes with inherent intelligence. In the late 1980s, Japanese researchers firstly introduced the idea of smart cementitious materials [10,11]. The 'smartness' of cementitious materials is characterized by their capabilities such as self–sensing, self–adapting, self–heating, self–cleaning and so on [12]. These intelligent properties are typical achieved through specialized processing techniques, modification of material composition and microstructures and introduction of other functional elements [9]. For instance, intrinsic

self–sensing cementitious materials can be created through the incorporation of suitable electrically active additives [6,7]. These additives can take various forms such as carbon nanotube, conductive sheets, carbon fiber, and metal powder [13–17].

As the focus on smart cementitious materials increases, the methods for predicting their mechanical performance warrant further investigation. Nonetheless, the complex microstructures and functional components of these materials present a considerable challenge in the development of analytical models or empirical equations. Additionally, it is expensive and time–consuming to conduct experimental tests on cementitious composites to assess their properties. A potential solution could be the utilization of data–driven methods, that is, machine learning (ML), to formulate prediction models for smart cementitious materials. Indeed, multiple MI methods have recently been employed to evaluate the properties of engineering materials. For instance, the random forest (RF) was utilized by Farooq et al. [18] to estimate the mechanical strength of quasi–brittle concrete and the results showed that good prediction can be achieved by the RF. Chou et al. [19] used multiple data–driven tools to estimate the uniaxial compressive strength of normal concrete, confirming that prediction with high accuracy can be provided by ML models. Both the RF method and the decision tree (DT) were used to forecast the strength of cementitious composites by Sohaib et al. [20] and it was shown that higher prediction accuracy can be achieved by the RF model. Moreover, extreme gradient boosting (XGB) algorithms was utilized by Li et al. [21] to estimate the properties of quasi–brittle materials with carbon nanotubes. The results indicated that the XGB technique can achieve superior performance in predicting the mechanical properties of quasi–brittle materials. Similar results have also been reported in [22,23].

The Artificial Neural Network (ANN) method has garnered significant attention as a predictive tool for material performance among numerous ML strategies. Saleh et al. [24] utilized ANN, nonlinear regression, Gaussian process regression, and multi–expression programming to estimate the performances of engineering cementitious composites. Their results indicated that higher accuracy can be achieved by the ANN model compared to other approaches. Similarly, the results reported in [25] showed that the neural network exhibits a superior performance in comparison with conventional regression methods in predicting the characteristics of carbon nanotubes modified by cement paste. In [26], Hu et al. utilized five machine learning tools to predict the triaxial properties of high–temperature treated rock. They found that the back propagation neural network (BPNN) exhibited a superior performance among the considered methods. These studies highlight the advantages of neural networks (NN) in estimating the mechanical properties and behaviors of materials. However, the initial weights and biases of NN are commonly determined by experience, resulting a low convergence speed and predictive accuracy. Also, poor capability for reproduction is found to be more common in the predictive models developed by traditional ANN, particularly when multiple input parameters are involved. To address this issue, this work introduces the particle swarm algorithm (one of the effective optimization algorithm) to optimize the ANN such that the initial parameters can be determined automatically, and then evaluates the performance of proposed PSO–BPNN algorithm for predicting the strength of smart cementitious materials for the first time, to the best knowledge of authors. The present results can help in developing models for accurate prediction of the properties of smart cementitious materials.

This paper is organized as follows. Section 2 present the particle swarm optimized back propagation neural network algorithm in detail. The developed prediction scheme is applied for two typical smart cementitious materials in Section 3. The training and testing results are presented and discussed. Finally, the conclusions and future work are drawn in Section 4.

2. Methodology

A PSO–BPNN algorithm is presented in this section for performance prediction of smart cementitious materials.

2.1. Back Propagation Neural Network

BPNN is a typical machine learning technique that uses a supervised learning method for training. The term 'back propagation' refers to the way by which the network learns from the error, that is, by propagating the error backwards and adjusting the weights and biases accordingly. Figure 1 presents a typical structure of the neural network.

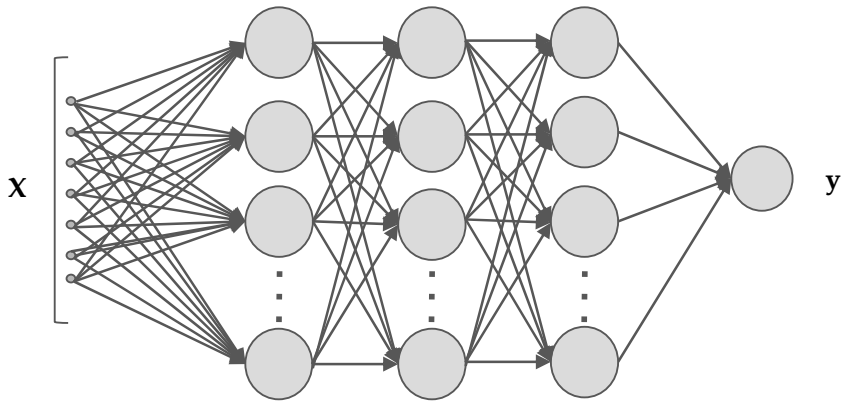

Figure 1. BPNN structure.

BPNN training comprises three primary stages: the forward propagation of data, the backward propagation of errors and the adjusting of weights and biases. During forward propagation, the data is fed into the input layer, and then passed to the output layer through the hidden layers. In the subsequent step, the error is computed and propagated back from the output layer to the input layer. Then, the weights and biases are adjusted accordingly to reduce the error level. This process would be repeated multiple times for all samples until the error level is minimized.

Specifically, during the data forward propagation, the net input $\mathbf{z}_i$ for layer i is calculated using the output $\mathbf{y}_{i-1}$ from layer $i-1$, and then the output $\mathbf{y}_i$ for layer i is determined by applying an activation function to $\mathbf{z}_i$ which is expressed as

$$\begin{cases} \mathbf{z}_i = \boldsymbol{\omega}_i \mathbf{y}_{i-1} + \mathbf{b}_i \\ \mathbf{y}_i = f_i(\mathbf{z}_i) \end{cases}, \tag{1}$$

for which $\boldsymbol{\omega}_i$ and $\mathbf{b}_i$ are the weight and bias matrix from layer $i-1$ to i, respectively; $f_i(\cdot)$ represents the activation function.

Backward propagation of error is a learning mechanism that adjusts the weights and bias of neural networks to optimize the prediction performance. For a data point $(\mathbf{x}, \mathbf{y})$ put into the BPNN with an output of $\hat{\mathbf{y}}$, the error for layer i is calculated by

$$\boldsymbol{\delta}_i = \frac{\partial g(\mathbf{y}, \hat{\mathbf{y}})}{\partial \mathbf{z}_i} = f_i'(\mathbf{z}_i) \otimes \left({\boldsymbol{\omega}_i}^{\mathrm{T}} \boldsymbol{\delta}_{i-1} \right), \tag{2}$$

where $g(\mathbf{y}, \hat{\mathbf{y}})$ is the loss function; $(\cdot)^{\mathrm{T}}$ is the matrix transpose operator; $f_i'(\cdot)$ represents the derivative of the activation function; and $\otimes$ denotes the dot product operator of the vector, indicating that each element is multiplied by its corresponding element.

Once the error is propagated from the output layer to the input layer through the hidden layer, the weight and bias matrix for each layer can be updated accordingly, that is

$$\begin{cases} \boldsymbol{\omega}_i \leftarrow \boldsymbol{\omega}_i - \alpha \left(\boldsymbol{\delta}_i \mathbf{y}_i^{\mathrm{T}} + \lambda \boldsymbol{\omega}_i \right) \\ \mathbf{b}_i \leftarrow \mathbf{b}_i - \alpha \boldsymbol{\delta}_i \end{cases}, \tag{3}$$

together with the learning rate α and regularization factor λ.

BPNN is widely used in many applications due to its ability to learn complex patterns and relationships in data. When building a performance prediction model for smart

cementitious materials, the following steps are commonly involved: (1) collecting training and test data sets; (2) setting the structure of neural network and configuring model parameters; (3) training the network using the training dataset; (4) validating the network using the test dataset; (5) evaluating the predictive performance. It should be emphasized that the effectiveness of training a BPNN is heavily dependent on the initial parameters, which include the weights and biases. The random selection of initial parameters in the traditional BPNN restricts its practical application.

2.2. Particle Swarm Optimization Algorithm

Particle Swarm Optimization (PSO) is a global random optimization method that relies on a population–based strategy. It was initially put forward by Kennedy and Eberhart [27]. PSO defines a group of potential problem solutions as a swarm of particles that can navigate the problem space driven based on their own and nearby particles' best performance, enabling the achievement of an optimal solution. Algorithm 1 gives the detailed computational scheme of the PSO algorithm [28].

Algorithm 1 Particle swarm optimization

1. Initialization. For each of the N particles:
a. Initialize the position and velocity $\mathbf{x}_i(0)$ and $\mathbf{v}_i(0)$ $\forall i \in 1:N$;
b. Initialize the particle's own best position $\mathbf{p}_i(0) = \mathbf{x}_i(0)$;
c. Compute the fitness value of each particle and if $f\left(\mathbf{x}_j(0)\right) \geq f(\mathbf{x}_i(0))$ $\forall i \neq j$, initialize the global best solution as $\mathbf{g} = \mathbf{x}_j(0)$;
2. Repeat the following steps until the termination condition is met:
a. Update the particle velocity using the following equation:
$\mathbf{v}_i(t+1) = \omega \mathbf{v}_i(t) + c_1 R_1(\mathbf{p}_i - \mathbf{x}_i(t)) + c_2 R_2(\mathbf{g} - \mathbf{x}_i(t))$;
b. Update the particle position using the following equation:
$\mathbf{x}_i(t+1) = \mathbf{x}_i(t) + \mathbf{v}_i(t+1)$;
c. Compute the fitness value of each particle $f(\mathbf{x}_i(t+1))$;
d. If $f(\mathbf{x}_i(t+1)) \geq f(\mathbf{p}_i)$, update the personal best position: $\mathbf{p}_i = \mathbf{x}_i(t+1)$;
e. If $f(\mathbf{x}_i(t+1)) \geq f(\mathbf{g})$, update the personal best position: $\mathbf{g} = \mathbf{x}_i(t+1)$;
3. Output the optimal result.

Note that c_1 and c_2 in Table 1 are learning factors which are usually in the range of [0,4]; R_1 and R_2 represents two random variables which both satisfies a uniform probability distribution in [0,1]; and ω represents the inertia weight that is calculated by

$$\omega = \omega_{\max} - (\omega_{\max} - \omega_{\min}) \frac{N_c}{N_{\max}}, \tag{4}$$

together with a maximum inertia weight $\omega_{\max}$ and minimum inertia weight $\omega_{\min}$. In Equation (4), $N_{\max}$ is the total iteration number and N_c is the current iteration number. Equation (4) suggests that with an increase in the number of iterations, the inertia weight decreases progressively. This implies that during the initial stage, the PSO algorithm exhibits a strong global exploration capability, while in the later stage it demonstrates a robust local exploitation ability.

Table 1. Model parameters for the PSO algorithm.

N	c_1	c_2	$\omega_{\max}$	$\omega_{\min}$	$\text{iter}_{\max}$
10	2	2	0.9	0.4	50

2.3. PSO–BPNN

As previously illustrated, appropriate initial parameters can enhance the prediction performance of the BPNN as well as the learning speed. Therefore, we employ the PSO method to optimize the initial weights and biases, with the aim of improving prediction

accuracy and reducing learning time. Specifically, prior to the training of the neural network, the particle swarm optimization approach is utilized to initialize the weights and biases. The PSO search for the optimal positions by using the mean squared error of the network as the fitness function. The optimized parameters is subsequently allocated to the BPNN as the initial weights and biases. Algorithm 2 gives the detailed steps of the PSO–BPNN.

Algorithm 2 PSO-BPNN

1. Design the network structure and set the involved parameters;
2. Initialize the positions and velocities of particles and define the fitness function of the PSO algorithm;
3. Iterate using the PSO algorithm to locate the best positions;
4. Assign the optimized parameters to the BPNN;
5. Training and testing the prediction performance of the BPNN model in terms of accuracy and error

3. Application Examples and Discussions

In this section, the proposed PSO–BPNN algorithm is employed for predicting the strength of two typical smart cementitious materials, i.e., 3D printed fiber reinforced concrete (3DP–FRC) and grapheme nanoparticles–reinforced cementitious composites (GrN–CC) and relevant results are discussed. Note that a systematic review of relevant experimental studies were conducted from Google scholar and web of science databases and that satisfying the following criteria were included for data collecting: the selected studies were scientific papers online and the material composition and experimental conditions were clearly given.

A three–layer neural network is used for both examples. The learning rate α and regularization factor λ are set as 0.01 and 0.1, respectively. The initial parameters for the particle swarm optimization algorithm are shown in Table 1. In addition, a traditional BPNN with same structure and parameters is also utilized for the comparison of prediction accuracy and error.

Five widely used statistical metrics are applied to evaluate the predictive accuracy of the models, represented as Equations (5)–(9). A prediction model with a higher R^2 and lower MSE, MAE, MAPE and RMSE can be considered to exhibit a superior performance.

$$R^2 = 1 - \frac{\sum_{i=1}^{m} (y_i - \hat{y}_i)^2}{\sum_{i=1}^{m} (y_i - \overline{y})^2}, \tag{5}$$

$$\mathrm{MAE} = \frac{1}{m} \sum_{i=1}^{m} |y_i - \hat{y}_i|, \tag{6}$$

$$\mathrm{MSE} = \frac{1}{m} \sum_{i=1}^{m} (y_i - \hat{y}_i)^2, \tag{7}$$

$$\mathrm{RMSE} = \sqrt{\frac{1}{m} \sum_{i=1}^{m} (y_i - \hat{y}_i)^2}, \tag{8}$$

$$\mathrm{MAPE} = \frac{1}{m} \sum_{i=1}^{m} \frac{|y_i - \hat{y}_i|}{y_i}, \tag{9}$$

in which y_i denote the experimental data while $\hat{y}_i$ is the predicted value; $\overline{y}$ is the mean value; n is the sample number.

3.1. 3D Printed Fiber Reinforced Concrete

3.1.1. Data Collection and Description

Three dimensional printing technology, an additive manufacturing method, has been an important tool for the creation of smart materials and structures. Herein the proposed PSO–BPNN algorithm is employed to develop a predictive model for the compressive strength (CS) of 3DP–FRC.Thus, a total of 268 experimental values are collected from recently published articles [29–37]. Fifteen parameters, namely, water/binder ratio (W/B), ordinary Portland cement (OPC, kg/m^3), curing age (CA, days), water (W, kg/m^3), fly ash (FA, kg/m^3), sand (S, kg/m^3), fiber volume fraction (V_f, %), ground slag (GS, kg/m^3), hydroxypropyl methylcellulose (HPMC, kg/m^3), silica fume (SF, kg/m^3), superplasticizer (SP, kg/m^3), loading direction (LD), fiber length (Lf, mm), fiber diameter (Df, μm), and fiber type (F_{type}) are chosen as input variables. Accordingly, the number of neurons is configured as 15, 13 and 1 for each layer. Three loading directions are usually involved in the compressive experiments of 3D printed concrete, i.e., X, Y, Z. X denotes the direction parallel to the 3D printing direction which is marked as 1. Y and Z represent the perpendicular and vertical directions, and they are labeled as 2 and 3, respectively. Moreover, five types of fiber are included in the database: polyethylene (PE), steel, polyvinyl alcohol (PVA), polypropylene (PP) and basalt. They are labled as 1–5, respectively. To offer a comprehensive understanding for the collected dataset, six statistical parameters for the experimrntal dara are summarized in Table 2, including mean value, standard deviation, maximum value, minimum value, kurtosis and skewness. Kurtosis represents the symmetry of the variables, and skewness denotes whether the distribution of data is light–tailed or heavy–tailed in comparison with Gaussion distribution.

Table 2. The statistical parameters of the collected experimental data for 3DP–FRC.

Variables	Mean Value	Standard Deviation	Maximum Value	Minimum Value	Kurtosis	Skewness
OPC (kg/m^3)	534.00	194.92	1112.3	285.30	4.07	1.16
W/B	0.21	0.055	0.35	0.16	2.82	0.87
S (kg/m^3)	804.04	414.72	1902	246	2.61	0.10
FA (kg/m^3)	315.98	424.54	1141.4	0	1.96	0.81
GS (kg/m^3)	170.00	170.84	450	0	1.18	0.077
SF (kg/m^3)	182.46	128.41	377.80	0	1.71	−0.27
SP (kg/m^3)	6.98	4.95	20	0	2.47	0.43
HPMC (kg/m^3)	0.83	1.26	3.8	0	3.39	1.30
W (kg/m^3)	258.54	84.49	427.90	182	1.61	0.45
Vf (%)	0.01	0.0073	0.02	0	1.65	0.23
CA (days)	24.25	8.76	28	1	4.86	−1.94
LD (x, y, z)	2.14	0.81	3	1	1.56	−0.26
D_f (μm)	45.64	52.54	200	15	7.62	2.52
L_f (mm)	7.20	3.57	18	0	3.98	0.95
F_{type}	2.43	0.99	5	1	2.94	0.58
CS (MPa)	67.95	37.65	153.40	8	1.93	0.13

Further, it is crucial to standardize the data before fed into the neural network to ensure that all parameters are consistent and any potential bias can be prevented in the machine learning algorithms. In Matlab, the function *mapminmax* is utilized to scale the feature values within a specific range, and thereby the performance of the models can be enhanced. In addition, the data collected from the previous articles is divided into a training set containing 218 data points and a testing set containing 50 data points to build and assess the prediction model.

3.1.2. Results and Discussions

Figures 2 and 3 compare the prediction performance of BPNN and PSO–BPNN models on the training and testing datasets, respectively. It is shown that the prediction values of

the PSO–BPNN model follow the experimental values more closely than those of BPNN. It can be observed that PSO–BPNN provides predictions for nearly all samples within an error level of ±20% on the training set and an error level of ±10% on the testing dataset, which indicates that all predictions with PSO–BPNN match the experimental values reasonably well. The model errors in Figures 2b and 3b clearly show that the proposed PSO–BPNN algorithm yields less error and higher accuracy compared to the traditional BPNN model.

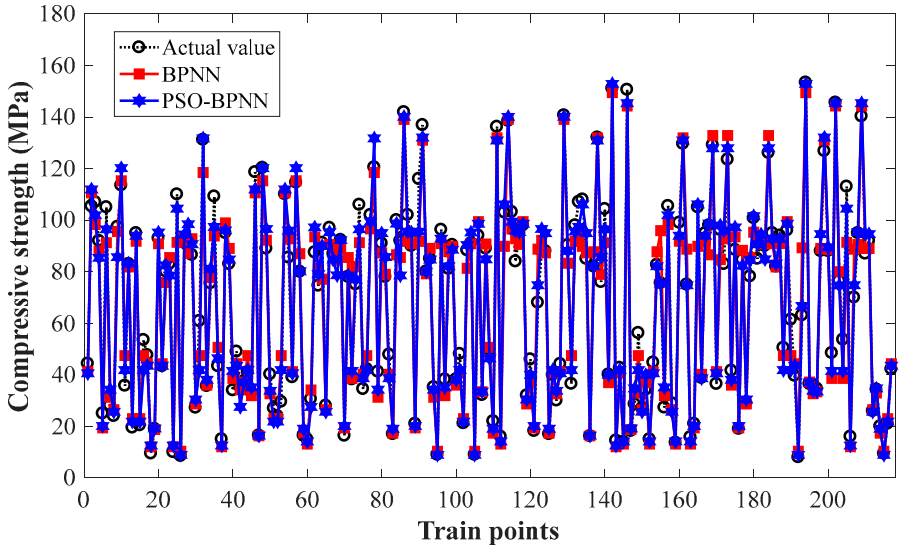

(**a**)

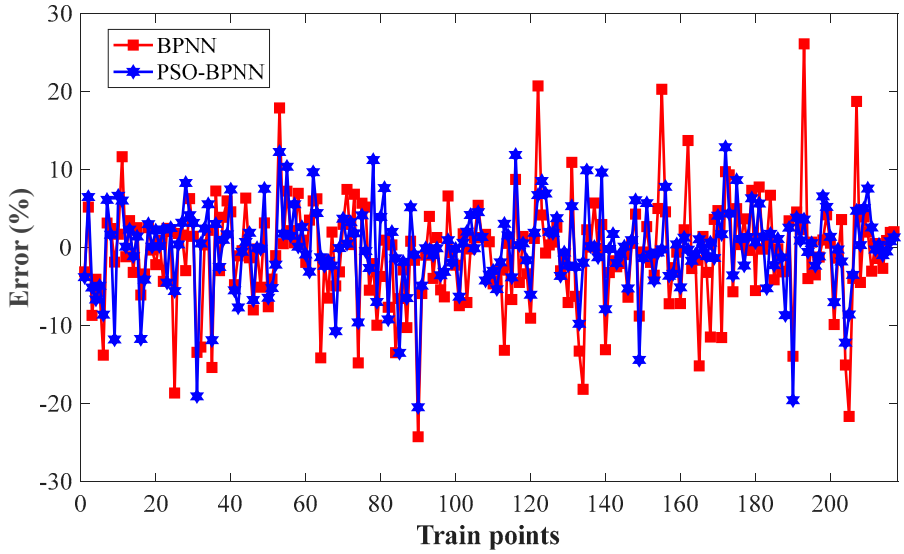

(**b**)

Figure 2. Prediction performance of BPNN and PSO-BPNN for the training set: (**a**) compressive strength of 3DP-FRC; (**b**) error analysis.

The regression slope is an effective tool for assessing the performance of machine learning models. In a regression plot, the prediction values are plotted against the experimental values. The regression slopes of the BPNN and PSO–BPNN models are depicted in Figures 4 and 5, respectively. As shown, the BPNN model yields a regression slope of 0.96 in training set and 0.91 in testing set, while the PSO–BPNN model obtains a regression slope of 0.99 and 0.97 for the corresponding sets, respectively. The regression slopes of the

PSO–BPNN model are closer to one compared to those of the BPNN model, indicating a better prediction performance.

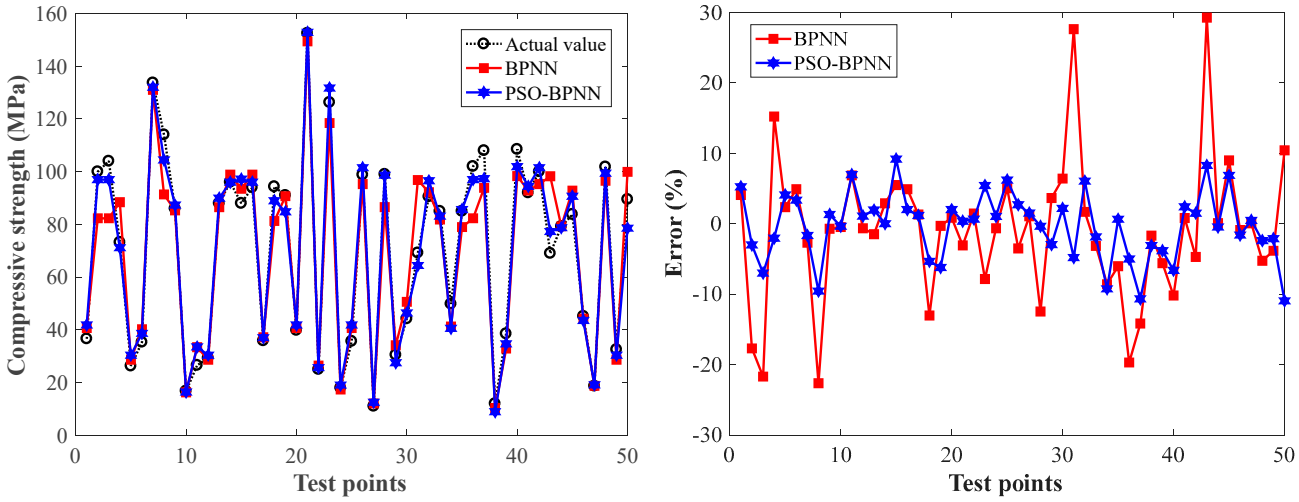

(**a**) (**b**)

Figure 3. Prediction performance of BPNN and PSO-BPNN for the testing set: (**a**) compressive strength of 3DP-FRC; (**b**) error analysis.

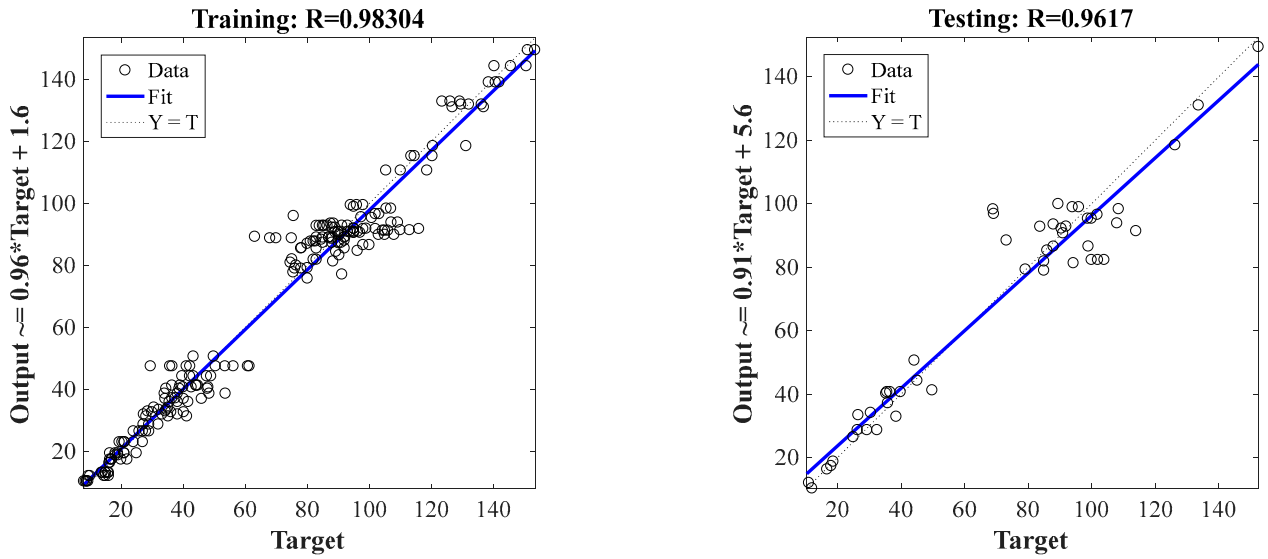

(**a**) (**b**)

Figure 4. Regression plots of BPNN for 3DP-FRC: (**a**) training set; (**b**) testing set.

Five statistical measures, i.e., R^2, MSE, MAE, MAPE and RMSE, are computed and summarized in Table 3. It can be observed that the PSO–BPNN model yields a higher index of R^2 and lower scores for MSE, MAPE, MAE and RMSE on the training dataset as well as the testing dataset compared to the BPNN model, which indicates that the proposed PSO–BPNN demonstrates a better performance for predicting the mechanical strength of 3D printed concrete. Moreover, the R^2 values of PSO–BPNN for training and testing are both 0.99, demonstrating its strong capability for generalization. The error indicators of PSO–BPNN are further improved on the testing dataset.

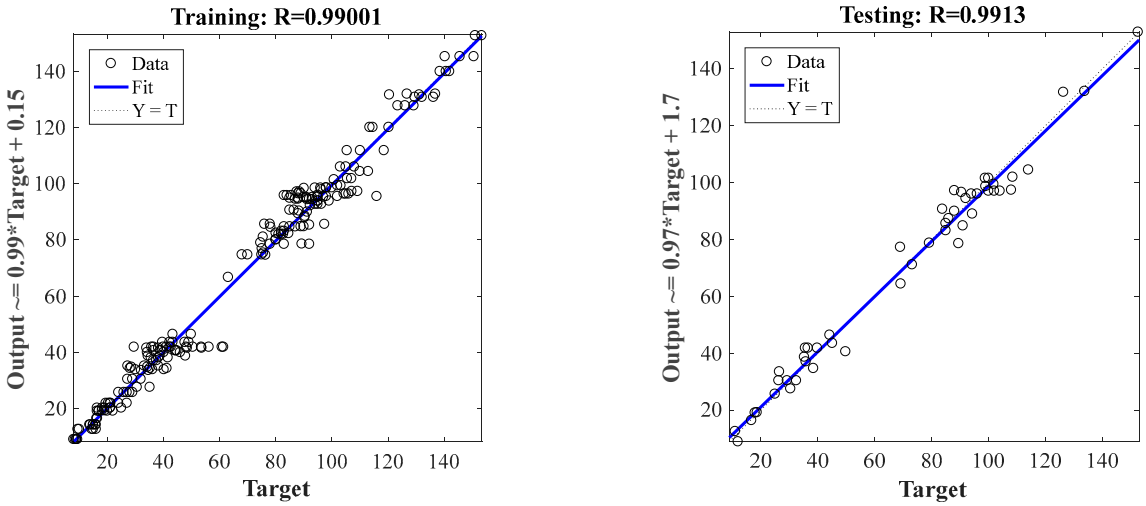

(**a**) (**b**)

Figure 5. Regression plots of PSO–BPNN for 3DP–FRC: (**a**) training set; (**b**) testing set.

Table 3. Various statistical parameters of the BPNN and PSO–BPNN models for 3DP–FRC.

Model	R^2	MAE	MSE	RMSE	MAPE
Training					
BPNN	0.98	5.03	49.25	7.02	8.97%
PSO–BPNN	0.99	4.86	28.95	5.38	7.25%
Testing					
BPNN	0.96	6.76	98.24	9.91	9.94%
PSO–BPNN	0.99	3.72	22.66	4.76	6.72%

In addition, Alyami et al. [38] have utilized the same experimental data to develop prediction models for compressive strength of 3D–FRC using various machine learning techniques, including support vector regression (SVR), decision tress (DT), random forest (RF), SVR–Bagging, gradient boosting (GB), SVR–Boosting and gene expression programming (GEP). Some statistical parameters for these models are provided in Table 4. The comparison between Tables 3 and 4 confirms that the proposed PSO–BPNN model exhibits a superior performance in predicting the strength of 3D–FRC.

Table 4. Various statistical parameters for the developed models in [38].

Model	*R*	MAE	RMSE
SVR	0.84	10.245	18.717
DT	0.987	4.644	6.589
RF	0.986	3.989	7.134
SVR–Bagging	0.897	10.771	19.007
GB	0.986	3.901	7.211
SVR–Boosting	0.961	9.491	12.833
GEP	0.985	5.691	6.405

3.2. Graphene Nanoparticles Reinforced Cementitious Composites

3.2.1. Data Collection and Description

Graphene nanoparticles reinforced cementitious composites (GrN–CC) have gained significant attention because of their improved physical, mechanical and crack–resistant properties. Nevertheless, the development of computational models for the properties of GrN–CC using conventional methods is quite challenging, due to their intricate multiscale structures. Now the proposed PSO–BPNN is utilized for the construction of a

prediction model for the compressive strength of GrN–CC. A series of experimental results is gathered from recently published articles [39–68] that consists of 172 data points for the CS of GrN–CC. Seven parameters, namely curing age (CA, days), sand content (SC), water/cement ratio (w/c), GrN diameter (GD, μm), GrN content (GC, wt%), GrN thickness (GT, nm) and ultrasonication (US, hr) are considered as input variables. Accordingly, a neural network of 7–11–1 is designed for the prediction model. Table 5 gives the statistical parameters for the collected experimental results to aid data comprehension. During data pre–processing, the data is standardized to prevent the potential bias in training. Moreover, the experimental data is also divided two subsets, i.e., a training data set consisting of 142 data points and a testing dataset consisting of 30 data points, to build and assess the prediction model, respectively.

Table 5. The statistical parameters of the collected experimental data for GrN–CC.

Variables	Mean Value	Standard Deviation	Maximum Value	Minimum Value	Kurtosis	Skewness
SC	1.37	1.49	3	0	−1.99	0.16
GD (μm)	3.38	6.87	50	0.07	35.55	5.60
GT (nm)	3.39	5.19	27.6	0.7	14.18	3.63
GC (wt%)	0.26	0.94	6.4	0.01	31.12	5.44
w/c	0.40	0.11	0.72	0.2	1.43	1.24
US (h)	0.49	0.82	3	0	4.66	2.37
CA (days)	19.70	10.82	28	1	−1.49	−0.62
CS (MPa)	48.51	19.10	94.26	14.59	−0.60	0.20

3.2.2. Results and Discussions

Figures 6 and 7 depict the prediction performance of BPNN and PSO–BPNN models on the training and testing datasets, respectively. As shown, the PSO–BPNN model exhibits a superior predictive performance compared to the traditional BPNN. The PSO–BPNN yields predictions for nearly all samples within a ±15% error range on the training dataset and a ±10% error range on the testing dataset, which demonstrates that the experimental and predictive values are agree well.

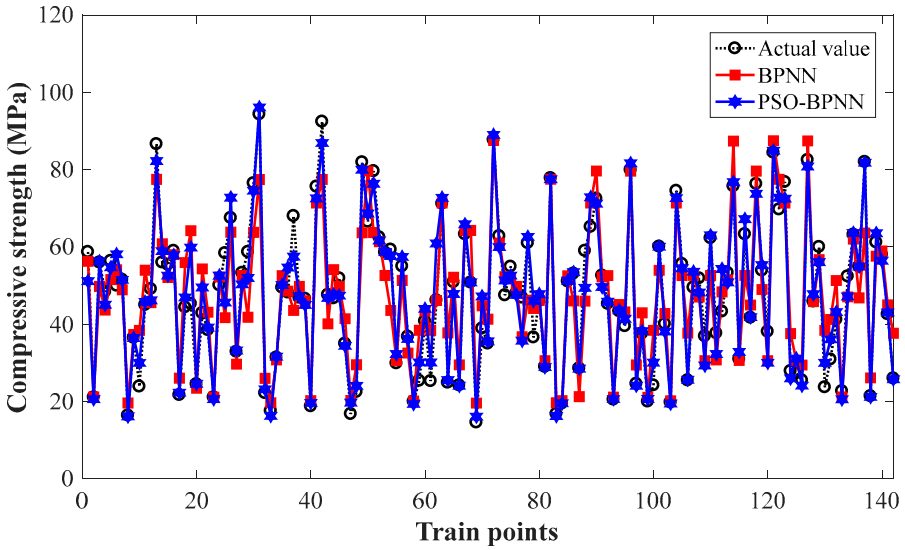

(**a**)

Figure 6. *Cont.*

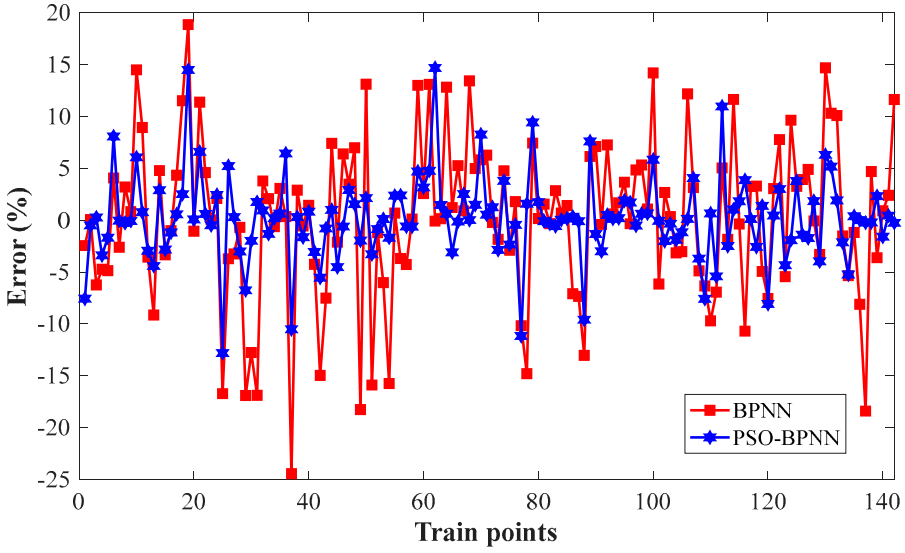

(**b**)

Figure 6. Prediction performance of BPNN and PSO–BPNN for the training set: (**a**) compressive strength of GrN–CC; (**b**) error analysis.

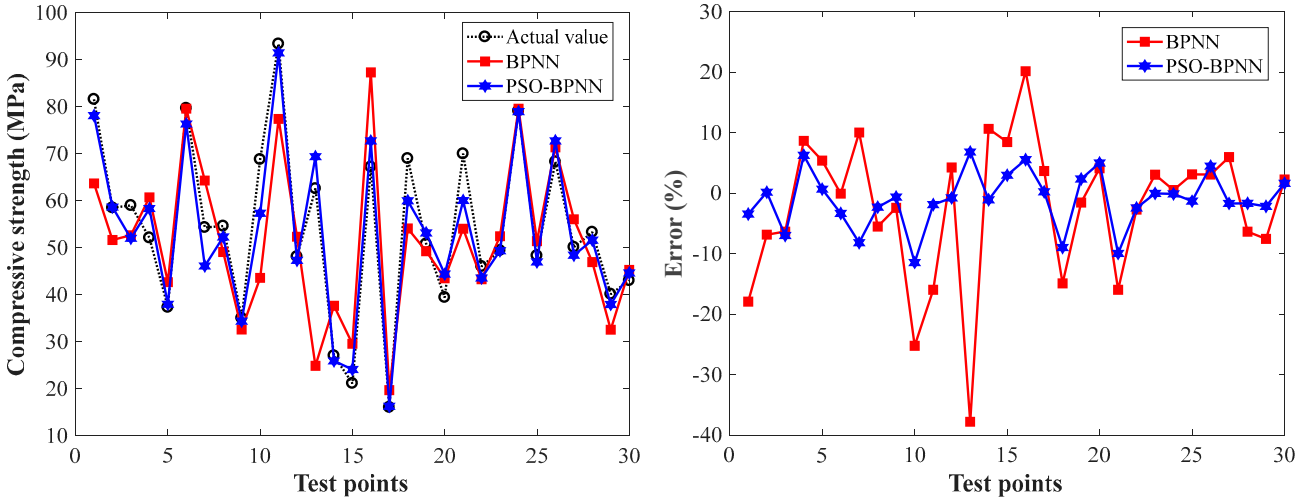

(**a**) (**b**)

Figure 7. Prediction performance of BPNN and PSO–BPNN for the testing set: (**a**) compressive strength of GrN–CC; (**b**) error analysis.

Figures 8 and 9 display the regression plots of the BPNN and PSO–BPNN predictive models, respectively. The BPNN model shows a regression slop of 0.81 for the training dataset and 0.7 for the testing dataset that is lower than the suggested threshold of 0.80, indicating a poor prediction performance. The PSO–BPNN model provides slops of 0.96 and 0.93 in training and testing, respectively. Once again, the ideal fit line confirms the reliability and robustness of the proposed PSO–BPNN algorithm.

Table 6 lists the quantitative indicators of BPNN and PSO–BPNN for both the training and testing datasets. The R^2 value of BPNN for training is 0.92 while for testing is just 0.77, indicating a poor performance for predicting the mechanical properties of GrN–CC. The R^2 value as well as the other error scores of PSO–BPNN are all in a reasonable range, which strongly suggests the excellent predictive performance of PSO–BPNN.

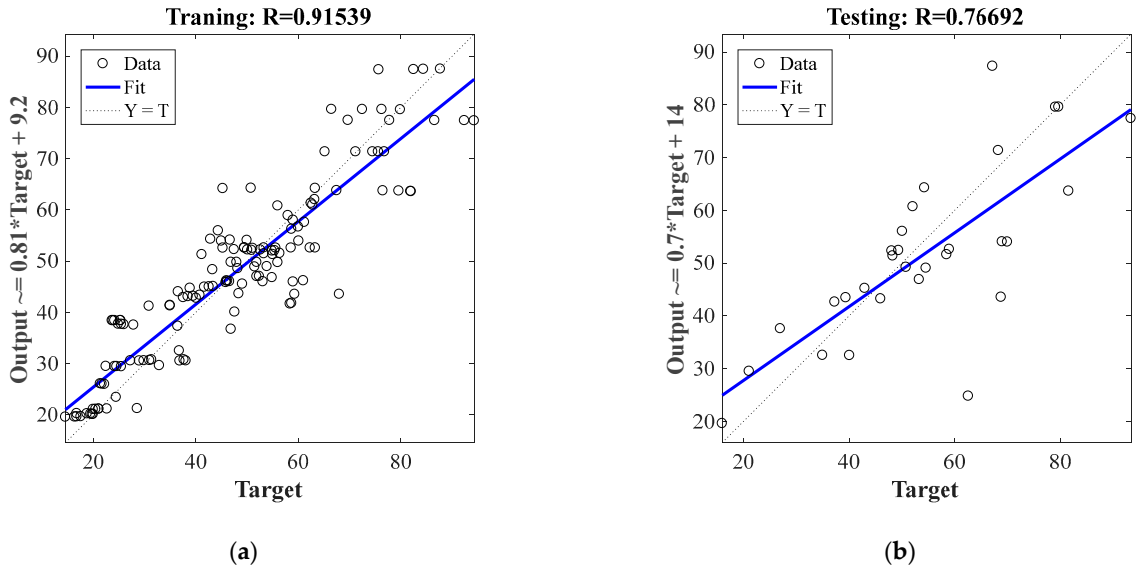

Figure 8. Regression plots of BPNN for GrN–CC: (**a**) training set; (**b**) testing set.

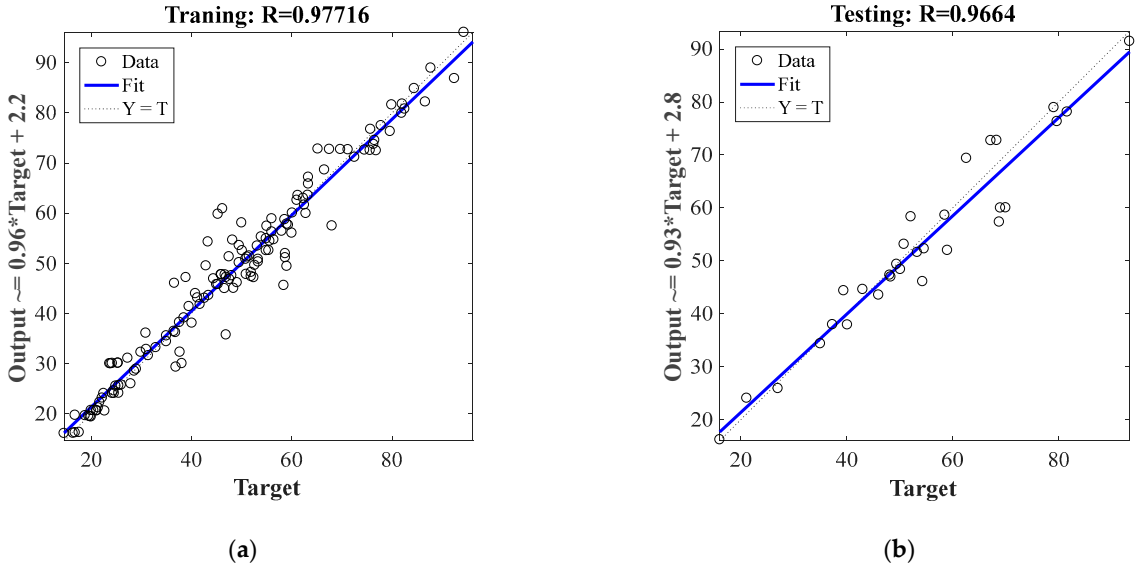

Figure 9. Regression plots of PSO-BPNN for GrN–CC: (**a**) training set; (**b**) testing set.

Table 6. Various statistical parameters of the BPNN and PSO−BPNN models for GrN−CC.

Model	R^2	MAE	MSE	RMSE	MAPE
Training					
BPNN	0.92	5.80	59.63	7.72	13.81%
PSO–BPNN	0.98	2.71	16.54	4.07	6.24%
Testing					
BPNN	0.77	8.68	141.91	11.91	16.51%
PSO–BPNN	0.97	3.49	21.96	4.69	6.32%

Table 7 gives the statistical parameters of the prediction models for the compressive strength of GrN–CC in [69] including the decision tree (DT), AdaBoost regressor (AR) and bagging regressor (BR) models. It can be seen from Tables 6 and 7 that the proposed PSO–BPNN models exhibit a superior predictive performance again.

Table 7. Various statistical parameters for the developed models in [69].

Model	*R*	MAE	RMSE
DT	0.87	4.60	5.44
AR	0.82	4.54	6.44
BR	0.80	5.42	6.73

4. Conclusions

Although the traditional back propagation neural network has been used in many studies for the prediction of material properties, its accuracy and robustness need further investigation. This work presents a back propagation neural network optimized by particle swarm algorithm (PSO–BPNN) for predicting the mechanical performance of smart cementitious materials. Specifically, the particle swarm method is introduced to determine the initial weights and bias such that the accuracy and robustness of neural network can be enhanced. The proposed algorithm is then applied to predict the mechanical strength of two typical smart cementitious materials, i.e., 3D printed fiber reinforced concrete and grapheme nanoparticles–reinforced cementitious composites. The results indicate that a performance prediction model with a high degree of accuracy and strong generalization capabilities can be developed using the PSO–BPNN methodology. Also, the comparative analysis demonstrates that the developed PSO–BPNN outperforms the traditional neural network in terms of the prediction accuracy, which means that the use of PSO–BPNN can provide more reliable and accurate predictions for the performance of smart cementitious materials.

The present findings of this work confirm the effectiveness of PSO–BPNN and can promote its use in predicting the mechanical properties of smart cementitious materials. However, the current study is built upon only two kinds of smart cementitous materials. More data for other smart materials should be gathered to validate the effectiveness of the PSO–BPNN method. In addition, other mechanical and physical properties, e.g., the shear strength, should be considered in future work. Finally, further research can investigate the performance of other popular soft computing techniques in improving the accuracy of BPNN.

Author Contributions: Conceptualization, F.K. and L.H.; Funding acquisition, F.K. and L.H.; Investigation, P.Z.; Methodology, P.Z. and L.H.; Software, P.Z.; Writing—original draft, P.Z.; Writing—review & editing, F.K. and L.H. All authors have read and agreed to the published version of the manuscript.

Funding: This research was funded by National Natural Science Foundation of China (52078399).

Data Availability Statement: Data are contained within the article, further inquiries can be directed to the corresponding author.

Acknowledgments: The financial support from National Natural Science Foundation of China is gratefully acknowledged.

Conflicts of Interest: The authors declare no conflicts of interest.

References

1. Larrard, F.D. *Concrete Mixture Proportioning: A Scientific Approach*; CRC Press: London, UK, 2014.
2. Han, B.; Sun, S.; Ding, S.; Zhang, L.; Yu, X.; Ou, J. Review of nanocarbon-engineered multifunctional cementitious composites. *Compos. Part A Appl. Sci. Manuf.* **2015**, *70*, 69–81. [CrossRef]
3. Huang, Y.; Zhang, H.; Zhou, J.; Xu, S. Efficient quasi-brittle fracture simulations of concrete at mesoscale using micro CT images and a localizing gradient damage model. *Comput. Meth. Appl. Mech. Eng.* **2022**, *400*, 115559. [CrossRef]
4. Hai, L.; Huang, Y.-J.; Wriggers, P.; Zhang, H.; Li, Q.-H. Investigation on fracture behaviour of UHPFRC using a mesoscale computational framework. *Comput. Meth. Appl. Mech. Eng.* **2024**, *421*, 116796. [CrossRef]
5. Li, Z.; Ding, S.; Yu, X.; Han, B.; Ou, J. Multifunctional cementitious composites modified with nano titanium dioxide: A review. *Compos. Part A Appl. Sci. Manuf.* **2018**, *111*, 115–137. [CrossRef]
6. Song, F.; Li, Q.; Xu, S. A review of self-sensing ultra-high performance concrete: Towards next-generation smart structural materials. *Cem. Concr. Compos.* **2024**, *145*, 105350. [CrossRef]

7. Li, W.; Qu, F.; Dong, W.; Mishra, G.; Shah, S.P. A comprehensive review on self-sensing graphene/cementitious composites: A pathway toward next–generation smart concrete. *Constr. Build. Mater.* **2022**, *331*, 127284. [CrossRef]
8. Makul, N. Advanced smart concrete—A review of current progress, benefits and challenges. *J. Clean Prod.* **2020**, *274*, 122899.
9. Han, B.; Wang, Y.; Dong, S.; Zhang, L.; Ding, S.; Yu, X.; Ou, J. Smart concretes and structures: A review. *J. Intell. Mater. Syst. Struct.* **2015**, *26*, 1303–1345. [CrossRef]
10. Chen, P.-W.; Chung, D.D.L. Carbon fiber reinforced concrete for smart structures capable of non-destructive flaw detection. *Smart Mater. Struct.* **1993**, *2*, 22.
11. Kamila, S. Introduction, classification and applications of smart materials: An overview. *Am. J. Appl. Sci.* **2013**, *10*, 876–880. [CrossRef]
12. Mishra, D.; Yu, J.; Das, A.K.; Leung, C.K. A review of self-sensing and self-healing 'smart'cement based materials-bridging the gap between research and adoption. In Proceedings of the 4th International Conference on Service Life Design for Infrastructures, Delft, The Netherlands, 27–30 August 2018.
13. Konsta–Gdoutos, M.S.; Aza, C.A. Self sensing carbon nanotube (CNT) and nanofiber (CNF) cementitious composites for real time damage assessment in smart structures. *Cem. Concr. Compos.* **2014**, *53*, 162–169. [CrossRef]
14. Han, B.; Ding, S.; Yu, X. Intrinsic self-sensing concrete and structures: A review. *Measurement* **2015**, *59*, 110–128. [CrossRef]
15. Dong, W.; Li, W.; Tao, Z.; Wang, K. Piezoresistive properties of cement–based sensors: Review and perspective. *Constr. Build. Mater.* **2019**, *203*, 146–163. [CrossRef]
16. Wang, L.; Aslani, F. A review on material design, performance, and practical application of electrically conductive cementitious composites. *Constr. Build. Mater.* **2019**, *229*, 116892. [CrossRef]
17. Wang, X.; Cao, B.; Vlachakis, C.; Al-Tabbaa, A.; Haigh, S.K. Characterization and piezo-resistivity studies on graphite-enabled self-sensing cementitious composites with high stress and strain sensitivity. *Cem. Concr. Compos.* **2023**, *142*, 105187. [CrossRef]
18. Farooq, F.; Nasir Amin, M.; Khan, K.; Rehan Sadiq, M.; Faisal Javed, M.; Aslam, F.; Alyousef, R. A comparative study of random forest and genetic engineering programming for the prediction of compressive strength of high strength concrete (HSC). *Appl. Sci.* **2020**, *10*, 7330. [CrossRef]
19. Chou, J.-S.; Chiu, C.-K.; Farfoura, M.; Al-Taharwa, I. Optimizing the prediction accuracy of concrete compressive strength based on a comparison of data-mining techniques. *J. Comput. Civil. Eng.* **2011**, *25*, 242–253. [CrossRef]
20. Nazar, S.; Yang, J.; Amin, M.N.; Khan, K.; Javed, M.F.; Althoey, F. Formulation of estimation models for the compressive strength of concrete mixed with nanosilica and carbon nanotubes. *Dev. Built Environ.* **2023**, *13*, 100113. [CrossRef]
21. Li, Y.; Li, H.; Jin, C.; Shen, J. The study of effect of carbon nanotubes on the compressive strength of cement-based materials based on machine learning. *Constr. Build. Mater.* **2022**, *358*, 129435. [CrossRef]
22. Nguyen-Sy, T.; Wakim, J.; To, Q.-D.; Vu, M.-N.; Nguyen, T.-D.; Nguyen, T.-T. Predicting the compressive strength of concrete from its compositions and age using the extreme gradient boosting method. *Constr. Build. Mater.* **2020**, *260*, 119757. [CrossRef]
23. Uddin, M.N.; Ye, J.; Deng, B.; Li, L.; Yu, K. Interpretable machine learning for predicting the strength of 3D printed fiber-reinforced concrete (3DP–FRC). *J. Build. Eng.* **2023**, *72*, 106648. [CrossRef]
24. Saleh, P.Y.; Jaf, D.K.I.; Abdalla, A.A.; Ahmed, H.U.; Faraj, R.H.; Mahmood, W.; Mohammed, A.S. Prediction of the compressive strength of strain-hardening cement-based composites using soft computing models. *Struct. Concr.* **2023**, *24*, 6761–6777. [CrossRef]
25. Piro, N.S.; Mohammed, A.S.; Hamad, S.M. Multiple analytical models to evaluate the impact of carbon nanotubes on the electrical resistivity and compressive strength of the cement paste. *Sustainability* **2021**, *13*, 12544. [CrossRef]
26. Hu, X.; Shentu, J.; Xie, N.; Huang, Y.; Lei, G.; Hu, H.; Guo, P.; Gong, X. Predicting triaxial compressive strength of high-temperature treated rock using machine learning techniques. *J. Rock Mech. Geotech. Eng.* **2023**, *15*, 2072–2082. [CrossRef]
27. Kennedy, J.; Eberhart, R. Particle swarm optimization. In Proceedings of the ICNN'95—International Conference on Neural Networks, Perth, WA, Australia, 27 November–1 December 1995; Volume 4, pp. 1942–1948.
28. Marini, F.; Walczak, B. Particle swarm optimization (PSO). A tutorial. *Chemom. Intell. Lab. Syst.* **2015**, *149*, 153–165. [CrossRef]
29. Ma, G.; Li, Z.; Wang, L.; Wang, F.; Sanjayan, J. Mechanical anisotropy of aligned fiber reinforced composite for extrusion-based 3D printing. *Constr. Build. Mater.* **2019**, *202*, 770–783. [CrossRef]
30. Ding, T.; Xiao, J.; Zou, S.; Zhou, X. Anisotropic behavior in bending of 3D printed concrete reinforced with fibers. *Compos. Struct.* **2020**, *254*, 112808. [CrossRef]
31. Van Der Putten, J.; Rahul, A.V.; De Schutter, G.; Van Tittelboom, K. Development of 3D printable cementitious composites with the incorporation of polypropylene fibers. *Materials* **2021**, *14*, 4474. [CrossRef] [PubMed]
32. Yu, J.; Leung, C.K.Y. Impact of 3D printing direction on mechanical performance of strain-hardening cementitious composite (SHCC). In Proceedings of the First RILEM International Conference on Concrete and Digital Fabrication—Digital Concrete, Zurich, Switzerland, 10–12 September 2018; pp. 255–265.
33. Arunothayan, A.R.; Nematollahi, B.; Ranade, R.; Bong, S.H.; Sanjayan, J.G.; Khayat, K.H. Fiber orientation effects on ultra-high performance concrete formed by 3D printing. *Cem. Concr. Res.* **2021**, *143*, 106384. [CrossRef]
34. Ye, J.; Cui, C.; Yu, J.; Yu, K.; Xiao, J. Fresh and anisotropic-mechanical properties of 3D printable ultra–high ductile concrete with crumb rubber. *Compos. Part B Eng.* **2021**, *211*, 108639. [CrossRef]
35. Pham, L.; Tran, P.; Sanjayan, J. Steel fibres reinforced 3D printed concrete: Influence of fibre sizes on mechanical performance. *Constr. Build. Mater.* **2020**, *250*, 118785. [CrossRef]

36. Yu, K.; McGee, W.; Ng, T.Y.; Zhu, H.; Li, V.C. 3D–printable engineered cementitious composites (3DP–ECC): Fresh and hardened properties. *Cem. Concr. Res.* **2021**, *143*, 106388. [CrossRef]
37. Pham, L.; Lin, X.; Gravina, R.J.; Tran, P. Influence of PVA and PP fibres at different volume fractions on mechanical properties of 3D printed concrete. In Proceedings of the 16th East Asian-Pacific Conference on Structural Engineering and Construction, Brisbane, Australia, 3–6 December 2019.
38. Alyami, M.; Khan, M.; Fawad, M.; Nawaz, R.; Hammad, A.W.A.; Najeh, T.; Gamil, Y. Predictive modeling for compressive strength of 3D printed fiber-reinforced concrete using machine learning algorithms. *Case Stud. Constr. Mater.* **2024**, *20*, e02728. [CrossRef]
39. Liu, J.; Fu, J.; Yang, Y.; Gu, C. Study on dispersion, mechanical and microstructure properties of cement paste incorporating graphene sheets. *Constr. Build. Mater.* **2019**, *199*, 1–11. [CrossRef]
40. Zhao, Y.; Liu, Y.; Shi, T.; Gu, Y.; Zheng, B.; Zhang, K.; Xu, J.; Fu, Y.; Shi, S. Study of mechanical properties and early-stage deformation properties of graphene-modified cement-based materials. *Constr. Build. Mater.* **2020**, *257*, 119498. [CrossRef]
41. Sun, H.; Ling, L.; Ren, Z.; Memon, S.A.; Xing, F. Effect of graphene oxide/graphene hybrid on mechanical properties of cement mortar and mechanism investigation. *Nanomaterials* **2020**, *10*, 113. [CrossRef] [PubMed]
42. Yang, H.; Monasterio, M.; Cui, H.; Han, N. Experimental study of the effects of graphene oxide on microstructure and properties of cement paste composite. *Compos. Part A Appl. Sci. Manuf.* **2017**, *102*, 263–272. [CrossRef]
43. Lv, S.; Ma, Y.; Qiu, C.; Sun, T.; Liu, J.; Zhou, Q. Effect of graphene oxide nanosheets of microstructure and mechanical properties of cement composites. *Constr. Build. Mater.* **2013**, *49*, 121–127. [CrossRef]
44. Metaxa, Z.S. Exfoliated graphene nanoplatelet cement-based nanocomposites as piezoresistive sensors: Influence of nanoreinforcement lateral size on monitoring capability. *Ciência Tecnol. Dos Mater.* **2016**, *28*, 73–79. [CrossRef]
45. Liu, Q.; Xu, Q.; Yu, Q.; Gao, R.; Tong, T. Experimental investigation on mechanical and piezoresistive properties of cementitious materials containing graphene and graphene oxide nanoplatelets. *Constr. Build. Mater.* **2016**, *127*, 565–576. [CrossRef]
46. Cao, M.; Zhang, H.; Zhang, C. Effect of graphene on mechanical properties of cement mortars. *J. Cent. South Univ.* **2016**, *23*, 919–925. [CrossRef]
47. Wang, Y.; Yang, J.; Ouyang, D. Effect of graphene oxide on mechanical properties of cement mortar and its strengthening mechanism. *Materials* **2019**, *12*, 3753. [CrossRef] [PubMed]
48. Sun, S.; Han, B.; Jiang, S.; Yu, X.; Wang, Y.; Li, H.; Ou, J. Nano graphite platelets-enabled piezoresistive cementitious composites for structural health monitoring. *Constr. Build. Mater.* **2017**, *136*, 314–328. [CrossRef]
49. Lv, S.; Liu, J.; Sun, T.; Ma, Y.; Zhou, Q. Effect of GO nanosheets on shapes of cement hydration crystals and their formation process. *Constr. Build. Mater.* **2014**, *64*, 231–239. [CrossRef]
50. Peng, H.; Ge, Y.; Cai, C.S.; Zhang, Y.; Liu, Z. Mechanical properties and microstructure of graphene oxide cement-based composites. *Constr. Build. Mater.* **2019**, *194*, 102–109. [CrossRef]
51. Bai, S.; Jiang, L.; Jiang, Y.; Jin, M.; Jiang, S.; Tao, D. Research on electrical conductivity of graphene/cement composites. *Adv. Cem. Res.* **2020**, *32*, 45–52. [CrossRef]
52. Wang, B.; Pang, B. Mechanical property and toughening mechanism of water reducing agents modified graphene nanoplatelets reinforced cement composites. *Constr. Build. Mater.* **2019**, *226*, 699–711. [CrossRef]
53. Sharma, S.; Kothiyal, N.C. Comparative Effects of pristine and ball-milled graphene oxide on physico-chemical characteristics of cement mortar nanocomposites. *Constr. Build. Mater.* **2016**, *115*, 256–268. [CrossRef]
54. Wang, B.; Jiang, R.; Wu, Z. Investigation of the mechanical properties and microstructure of graphene nanoplatelet-cement composite. *Nanomaterials* **2016**, *6*, 200. [CrossRef] [PubMed]
55. Zhai, S.; Pang, B.; Liu, G.; Zhang, Y.; Xu, K.; She, W.; Zhang, Y. Investigation on preparation and multifunctionality of reduced graphene oxide cement mortar. *Constr. Build. Mater.* **2021**, *275*, 122119. [CrossRef]
56. Papanikolaou, I.; Arena, N.; Al-Tabbaa, A. Graphene nanoplatelet reinforced concrete for self-sensing structures—A lifecycle assessment perspective. *J. Clean Prod.* **2019**, *240*, 118202. [CrossRef]
57. Ghazizadeh, S.; Duffour, P.; Skipper, N.T.; Bai, Y. Understanding the behaviour of graphene oxide in portland cement paste. *Cem. Concr. Res.* **2018**, *111*, 169–182. [CrossRef]
58. Wang, Q.; Wang, J.; Lu, C.; Liu, B.; Zhang, K.; Li, C. Influence of graphene oxide additions on the microstructure and mechanical strength of cement. *New Carbon Mater.* **2015**, *30*, 349–356. [CrossRef]
59. Liu, J.; Li, Q.; Xu, S. Reinforcing mechanism of graphene and graphene oxide sheets on cement-based materials. *J. Mater. Civ. Eng.* **2019**, *31*, 04019014. [CrossRef]
60. Wang, B.; Shuang, D. Effect of Graphene nanoplatelets on the properties, pore structure and microstructure of cement composites. *Mater. Express* **2018**, *8*, 407–416. [CrossRef]
61. Qureshi, T.S.; Panesar, D.K. Nano reinforced cement paste composite with functionalized graphene and pristine graphene nanoplatelets. *Compos. Part B Eng.* **2020**, *197*, 108063. [CrossRef]
62. Dalla, P.T.; Tragazikis, I.K.; Trakakis, G.; Galiotis, C.; Dassios, K.G.; Matikas, T.E. Multifunctional cement mortars enhanced with graphene nanoplatelets and carbon nanotubes. *Sensors* **2021**, *21*, 933. [CrossRef]
63. Du, H.; Pang, S.D. Enhancement of barrier properties of cement mortar with graphene nanoplatelet. *Cem. Concr. Res.* **2015**, *76*, 10–19. [CrossRef]

64. Lv, S.; Ting, S.; Liu, J.; Zhou, Q. Use of Graphene oxide nanosheets to regulate the microstructure of hardened cement paste to increase its strength and toughness. *CrystEngComm* **2014**, *16*, 8508–8516. [CrossRef]
65. Gong, K.; Pan, Z.; Korayem, A.H.; Qiu, L.; Li, D.; Collins, F.; Wang, C.M.; Duan, W.H. Reinforcing effects of graphene oxide on portland cement paste. *J. Mater. Civ. Eng.* **2015**, *27*, A4014010. [CrossRef]
66. Baomin, W.; Shuang, D. Effect and mechanism of graphene nanoplatelets on hydration reaction, mechanical properties and microstructure of cement composites. *Constr. Build. Mater.* **2019**, *228*, 116720. [CrossRef]
67. Zhang, N.; She, W.; Du, F.; Xu, K. Experimental study on mechanical and functional properties of reduced graphene oxide/cement composites. *Materials* **2020**, *13*, 3015. [CrossRef] [PubMed]
68. Tong, T.; Fan, Z.; Liu, Q.; Wang, S.; Tan, S.; Yu, Q. Investigation of the effects of graphene and graphene oxide nanoplatelets on the micro- and macro-properties of cementitious materials. *Constr. Build. Mater.* **2016**, *106*, 102–114. [CrossRef]
69. Khan, M.; Nassar, R.-U.-D.; Anwar, W.; Rasheed, M.; Najeh, T.; Gamil, Y.; Farooq, F. Forecasting the strength of graphene nanoparticles—Reinforced cementitious composites using ensemble learning algorithms. *Results Eng.* **2024**, *21*, 101837. [CrossRef]